

# CiFHER: A Chiplet-Based FHE Accelerator with a Resizable Structure

Sangpyo Kim\*, Jongmin Kim\*, Jaeyoung Choi\*, and Jung Ho Ahn\*

\*Seoul National University

gajh@snu.ac.kr

**Abstract**—Fully homomorphic encryption (FHE) is in the spotlight as a definitive solution for privacy, but the high computational overhead of FHE poses a challenge to its practical adoption. Although prior studies have attempted to design ASIC accelerators to mitigate the overhead, their designs require excessive amounts of chip resources (e.g., areas) to contain and process massive data for FHE operations.

We propose CiFHER, a chiplet-based FHE accelerator with a resizable structure, to tackle the challenge with a cost-effective multi-chip module (MCM) design. First, we devise a flexible architecture of a chiplet core whose configuration can be adjusted to conform to the global organization of chiplets and design constraints. The distinctive feature of our core is a recomposable functional unit providing varying computational throughput for number-theoretic transform (NTT), the most dominant function in FHE. Then, we establish generalized data mapping methodologies to minimize the network overhead when organizing the chips into the MCM package in a tiled manner, which becomes a significant bottleneck due to the technology constraints of MCMs. Also, we analyze the effectiveness of various algorithms, including a novel limb duplication algorithm, on the MCM architecture. A detailed evaluation shows that a CiFHER package composed of 4 to 64 compact chiplets provides performance comparable to state-of-the-art monolithic ASIC FHE accelerators with significantly lower package-wide power consumption while reducing the area of a single core to as small as 4.28mm<sup>2</sup>.

## I. INTRODUCTION

Privacy is no longer merely a virtue but a critical objective for corporates due to recently established strict data privacy policies, such as California Consumer Privacy Act (CCPA) and the EU General Data Protection Regulation (GDPR). For example, Apple’s App Tracking Transparency (ATT) policy cost technology companies \$15.8 billion in 2022 [64].

*Fully homomorphic encryption (FHE)* is emerging as an attractive solution providing strong privacy guarantees. FHE enables an unlimited number of computations directly on encrypted data without decryption; thus, it allows users to safely offload services without disclosing private information. Numerous studies have shown its applicability to practical privacy-preserving applications, including genomics [44], [55], biometrics [59], [75], and machine learning (ML) tasks [13], [23], [35], [60], [61].

There are two major competing classes of FHE based on the learning with errors (LWE) computational problem: one based on the ring LWE variant (e.g., BGV [14], BFV [15], [32], and CKKS [21] schemes) and the other based on the torus LWE (e.g., FHEW [30] and TFHE [22] schemes). This work focuses on the former class and, specifically, CKKS [21],

which stands out among the state-of-the-art FHE schemes due to its relatively high performance [8] and the ability to encrypt complex vectors. Such benefits make CKKS suitable for numerous practical tasks and, in particular, ML tasks.

Still, alleviating the computational and memory overhead of FHE is a challenging prerequisite for the widespread use of FHE because FHE workloads run over 10,000× slower than their unencrypted counterparts [51], [82]. To mitigate the overhead, prior work has attempted hardware acceleration [1], [10], [33], [50], [54], [57], [81], [82], [95]. In particular, ASIC FHE accelerator proposals [54], [57], [82] have achieved considerable performance enhancements. For example, ARK [54] can perform a CIFAR-10 CNN inference in 0.125 seconds with the ResNet-20 model, which takes 2,271 seconds in a single-threaded CPU implementation [60]. However, these remarkable speedups owe to the massive chip area usage (373.6–472.3mm<sup>2</sup>) that enables the deployment of unconventionally large on-chip memory capacity (256–512MB) and substantial amounts of computational logic.

As prior massive FHE accelerator designs are prohibitively costly to realize, we turn to the use of a *multi-chip module (MCM)*. The cost of a chip skyrockets with the die area in recent technology nodes due to severe degradation in yield and high design complexity [43], [85]. By splitting a monolithic chip design into several small *chiplets*, an MCM drastically reduces the cost and becomes a scalable solution in the post-Moore era. Abundant studies [7], [41], [63], [85], [89], [96], including commercial chips [68], [69], [72], [94], have demonstrated the efficiency of MCMs in high-performance computing (HPC).

We propose CiFHER, a flexible and cost-effective MCM architecture for FHE. First, we design a resizable chiplet core architecture. The resizing flexibility comes from our *recomposable number-theoretic transform (NTT) unit* that can provide varying computational throughput depending on the package configuration and technology demands. CiFHER’s resizable structure enables architects to split a monolithic design into multiple cores with a best-fit size for a given die area budget.

Given the architecture of a chiplet, we construct efficient package configurations of CiFHER, focusing on minimizing the high network cost of MCMs. Due to the technical constraints of a *network on package (NoP)* connecting chiplets, an MCM architecture becomes bottlenecked by the NoP communication between the cores; data communication has been a source of bottleneck even in prior monolithic accelerators, and the

MCM intensifies the problem. We resolve the problem by developing generalized data mapping methodologies optimized for the many-core MCM architecture. We also devise a *limb duplication* algorithm, which significantly reduces data communication during *base conversion (BConv)*, the second most dominant function in FHE.

Based on the analysis, we discover balanced combinations of the individual chiplet design, data mapping, and FHE algorithms under various design constraints. By collaboration of these contributions, CiFHER achieves comparable performance to prior monolithic chips; a CiFHER package with 16 cores performs an encrypted CIFAR-10 CNN inference using the ResNet-20 model [60] in 0.189 seconds. Depending on the area budget, CiFHER provides various core configurations, ranging from four 47.08mm<sup>2</sup> core dies to 64 4.28mm<sup>2</sup> core dies in default settings.

Overall, this work makes the following key contributions:

- To the best of our knowledge, CiFHER is the first FHE accelerator proposal that exploits MCMs to minimize the area of a single die.
- We design a flexible chiplet core with a recomposable NTT unit, which allows the distribution of memory and compute resources across multiple dies while taking advantage of the vector NTT unit.
- We introduce generalized data mapping methodologies on a tiled FHE accelerator to resolve the NoP communication bottleneck of MCMs.
- We propose limb duplication, an algorithmic optimization tailored to the MCM design, reducing the amount of die-to-die communication, which would have caused significant latency and energy overhead.

## II. BACKGROUND & MOTIVATION

### A. Fully Homomorphic Encryption (FHE)

*Homomorphic encryption (HE)* is classified into *leveled HE (LHE)* and *fully HE (FHE)* depending on the problem size. LHE supports only a limited number of operations (ops) and is usually used in conjunction with other cryptographic protocols, such as multi-party computation (MPC) [40], [52], to overcome the limitation. However, this approach incurs heavy user-side computation and data communication overhead. In contrast, FHE solely supports an unlimited number of ops.

The defining feature of FHE is *bootstrapping*. The LWE problem [77], which forms the cryptographic basis for state-of-the-art HE schemes, relies on the error in encryption for its security. When performing *HE ops* on encrypted data, the magnitude of errors increases and can threaten the data integrity without proper management. Bootstrapping reduces the magnitude of errors, thereby enabling more HE ops to be performed. In a typical FHE use case, a bootstrapping op is inserted after every predetermined number of HE ops is applied to the encrypted data.

### B. CKKS FHE Scheme

We explain the CKKS FHE scheme, the main target of this paper, in detail. During CKKS encryption, a (vector) *message*

composed of  $n$  numbers is first *packed* into a degree- $(N-1)$  integer polynomial referred to as *plaintext*, which is an element of a cyclotomic polynomial ring  $\mathcal{R}_Q = \mathbb{Z}_Q[X]/(X^N + 1)$  with the *degree*  $N \geq 2n$  and the *modulus*  $Q$ . In  $\mathcal{R}_Q$ , all integer ops are performed modulo  $Q$ .

A plaintext is *encrypted* into a *ciphertext* composed of two polynomials in  $\mathcal{R}_Q$ . We denote polynomials with bold characters (e.g.,  $\mathbf{v}$ ), and ciphertexts encrypting polynomials with brackets ( $[\mathbf{v}]$ ). Then, the encryption of  $\mathbf{v}$  can be formulated as Eq. 1;  $\mathbf{a}$  is a random polynomial in  $\mathcal{R}_Q$ ,  $\mathbf{s}$  is the *secret*, and  $\mathbf{e}$  is a (ring LWE) *error*.  $\mathbf{a}$  and  $\mathbf{b}$  can be disclosed to any entity without revealing  $\mathbf{v}$  or the message packed into  $\mathbf{v}$ .

$$[\mathbf{v}] = (\mathbf{a}, \mathbf{b}) \in \mathcal{R}_Q^2, \quad \mathbf{b} = \mathbf{a} \cdot \mathbf{s} + \mathbf{v} + \mathbf{e} \quad (1)$$

For decryption, the user evaluates  $\mathbf{b} - \mathbf{a} \cdot \mathbf{s}$  with the secret  $\mathbf{s}$  to get  $\mathbf{v} + \mathbf{e}$ . As an error  $\mathbf{e}$  is included in the output, the message is multiplied with a *scale*  $\Delta$  before encryption. Typically,  $\Delta$  is around  $2^{30}$ – $2^{60}$ . As far as the magnitude of error is much smaller than  $\Delta$ ,  $\mathbf{v}$  can be recovered.

In FHE circumstances, high  $N$  around  $2^{15}$ – $2^{17}$  and  $Q$  as large as  $2^{1500}$  are utilized to meet security constraints [6], [27]. CKKS utilizes the *residue number system (RNS)* to handle the large  $Q$  [20].  $Q$  is set to the product of  $L$  number of small primes ( $q_i$ 's), such that  $Q = \prod_{i=1}^L q_i$ . Then, each coefficient  $c$  of a polynomial is represented by an  $L$ -tuple of small *residues* ( $c \bmod q_1, \dots, c \bmod q_L$ ). Using RNS, a modulo- $Q$  integer op between large coefficients is replaced by a set of pairwise modulo- $q_i$  integer ops between the small residues.

The following is a list of *primitive HE ops* of CKKS. The list is not comprehensive but includes the most dominant HE ops. Primitive HE ops are building blocks of more sophisticated HE ops.  $[\mathbf{v}_1] = (\mathbf{a}_1, \mathbf{b}_1)$ ,  $[\mathbf{v}_2] = (\mathbf{a}_2, \mathbf{b}_2)$ .

- $\text{HAdd}([\mathbf{v}_1], [\mathbf{v}_2]) = (\mathbf{a}_1 + \mathbf{a}_2, \mathbf{b}_1 + \mathbf{b}_2) \rightarrow [\mathbf{v}_1 + \mathbf{v}_2]$ : evaluates element-wise addition (add) between (vector) messages.
- $\text{HMult}([\mathbf{v}_1], [\mathbf{v}_2]) = (\mathbf{a}_1 \cdot \mathbf{b}_2 + \mathbf{a}_2 \cdot \mathbf{b}_1, \mathbf{b}_1 \cdot \mathbf{b}_2) + \text{KS}(\mathbf{a}_1 \cdot \mathbf{a}_2, \text{evk}_\times) \rightarrow [\mathbf{v}_1 \cdot \mathbf{v}_2]$ : evaluates element-wise multiplication (mult) between messages.
- $\text{HRot}([\mathbf{v}_1], r) = (\mathbf{0}, \phi_r(\mathbf{b}_1)) + \text{KS}(\phi_r(\mathbf{a}_1), \text{evk}_r) \rightarrow [\phi_r(\mathbf{v}_1)]$ : evaluates cyclic rotation of the message by an integer  $r$ , called rotation amount.
- $\text{PMult}([\mathbf{v}_1], \mathbf{v}_2) = (\mathbf{a}_1 \cdot \mathbf{v}_2, \mathbf{b}_2 \cdot \mathbf{v}_2) \rightarrow [\mathbf{v}_1 \cdot \mathbf{v}_2]$ : similar to  $\text{HMult}$ , but  $\mathbf{v}_2$  is not encrypted.
- $\text{KS}(\mathbf{v}, \text{evk})$ : key-switching
- $\text{RS}([\mathbf{v}_1]) = (\mathbf{a}_1/\Delta, \mathbf{b}_1/\Delta) \rightarrow [\mathbf{v}_1/\Delta]$ : rescaling

Here,  $\phi_r$  is an *automorphism* in  $\mathcal{R}_Q$ ;  $\phi_r(\mathbf{v})$  is a polynomial whose coefficients are in a permuted order from  $\mathbf{v}$ . When performing mult or automorphism, as in  $\text{HMult}$  or  $\text{HRot}$ , terms such as  $\mathbf{s}^2$  or  $\phi_r(\mathbf{s})$  are produced. *Key-switching* (KS) eliminates such terms by a complex sequence of ops involving *evaluation keys* ( $\text{evk}_s$ ), which are special public keys encrypting  $\mathbf{s}^2$  ( $\text{evk}_\times$ ) or  $\phi_r(\mathbf{s})$  ( $\text{evk}_r$ ).

Meanwhile, the output ciphertext  $[\mathbf{v}_1 \cdot \mathbf{v}_2]$  produced by  $\text{HMult}$  or  $\text{PMult}$  is associated with the scale  $\Delta^2$  due to mult. *Rescaling* (RS) reduces the scale back to  $\Delta$  by dividing the ciphertext by  $\Delta$ . When using RNS, instead of dividing the polynomial by

$\Delta$ , we set  $q_i$ 's close to  $\Delta$  and instead divide by the last prime  $q_L$ . After rescaling, the modulus becomes  $Q/q_L$  and only primes  $q_1, \dots, q_{L-1}$  are utilized afterwards. Rescaling can be repeated for each prime until the modulus becomes  $q_1$ , where we need to perform bootstrapping to restore the modulus. Therefore, in CKKS, a polynomial is represented as an  $\ell \times N$  matrix ( $1 \leq \ell \leq L$ ) when  $\ell$  number of primes are currently utilized, which we denote  $\mathbf{v} \in \mathcal{R}_{Q_\ell}$  for  $Q_\ell = \prod_{i=1}^{\ell} q_i$ . Each row of the matrix corresponding to  $q_i$  is referred to as *limb*; a limb is a polynomial in  $\mathcal{R}_{q_i} = \mathbb{Z}_{q_i}[X]/(X^N + 1)$ .

### C. Primary Functions of CKKS

We defer a more detailed explanation of each HE op to prior work [11], [20], [21], [36] and instead break down HE ops into *primary functions* to discuss their computational aspects. **Number-theoretic transform (NTT)**: To reduce the complexity of a polynomial mult, NTT is utilized. A polynomial mult in  $\mathcal{R}_{q_i}$  is equivalent to a negacyclic convolution between the coefficients. NTT, a type of discrete Fourier transform, and its inverse (iNTT) are defined for each  $q_i$ . (i)NTT reduces the overall complexity of the convolution into  $O(N \log N)$  for each limb by adopting a fast Fourier transform (FFT) algorithm [25]. **Base conversion (BConv)**: A binary function between two polynomials requires them to use the same modulus; otherwise, BConv is required. For instance, evks use an *auxiliary modulus*  $P = \prod_{i=1}^K p_i$  along with  $Q_\ell$  ( $\mathcal{R}_{PQ_\ell}$ ). During key-switching, limbs corresponding to  $p_i$ 's for the input polynomial  $\mathbf{v} \in \mathcal{R}_{Q_\ell}$  are produced by BConv. 96% of BConv computation is spent on a matrix-matrix mult between a pre-computed *BConv table* (a  $K \times \ell$  matrix) and  $\mathbf{v}$  (an  $\ell \times N$  matrix) [54]. The resulting  $K \times N$  matrix is a polynomial in  $\mathcal{R}_P$ , which we combine with the original  $\mathbf{v}$  to obtain the final result in  $\mathcal{R}_{PQ_\ell}$ , having the same modulus as the evk.

**Automorphism ( $\phi_r$ )**: As discussed in Section II-B, automorphism is a data permutation function. The  $i$ -th coefficient of a polynomial is mapped to the  $(i \cdot 5^r \bmod N)$ -th position.

FHE computations are extremely expensive. The main contributor to the high computational cost is key-switching, which is a complex procedure involving multiple (i)NTTs and BConvs. As a result, (i)NTT and BConv account for more than 80% of the total computations in CKKS [54], [57]. Therefore, enhancing (i)NTT and BConv performance is the essence of FHE acceleration. Automorphism and basic element-wise functions, such as element-wise add and mult, account for the rest of the computations.

### D. Previous ASIC FHE Accelerators

F1 [81] is the first ASIC acceleration work to report bootstrapping performance. However, F1 targets small parameters of  $N = 2^{14}$  and  $L = 16$ , which only partially support bootstrapping. Later accelerator proposals, BTS [57], CraterLake [82], and ARK [54], fully support bootstrapping by targeting larger parameters of  $N = 2^{16}$ – $2^{17}$  and  $L = 24$ – $60$ . BTS places 2,048 processing elements (PEs) in a grid and connects them by global wires that span the whole chip. Each PE contains a *butterfly unit* for (i)NTT, a multiply-accumulate unit for BConv,

and a multiplier and an adder for element-wise functions. A butterfly unit is capable of performing the *butterfly ops* required in (i)NTT, which are shown in Eq. 2. ARK and CraterLake develop upon F1's design of placing  $\sqrt{N}$  parallel *lanes* in a cluster<sup>1</sup> that feeds data into massive *vector NTT units (NTTUs)*. A vector NTTU contains  $\frac{1}{2}\sqrt{N} \log N$  butterfly units, which are placed in an organization directly reflecting the four-step 2D FFT dataflow [9]. ARK deploys four NTTUs, and CraterLake 16.

$$\begin{aligned} \text{I. Butterfly}_{\text{NTT}}(a, b, w) &= (a + b \cdot w, a - b \cdot w) \\ \text{II. Butterfly}_{\text{iNTT}}(a, b, w) &= (a + b, (a - b) \cdot w) \end{aligned} \quad (2)$$

To tackle the increased number of computations and size of the working set when using large parameters, CraterLake, BTS, and ARK all rely on enormous amounts of computational logic and on-chip memory capacity; the latter even reaches 256–512MB. These designs end up using massive chip resources, utilizing a monolithic die sized 373.6–472.3mm<sup>2</sup> and dissipating up to 317W of power.

### E. Multi-Chip Module (MCM)

An MCM is a promising solution for scaling chips in the post-Moore era. By organizing a module with multiple small dies, referred to as *chipselets*, and connecting them using advanced packaging technologies providing high bandwidth on-package interconnects [16], [39], [65], MCMs reduce the area of an individual die. Because the design and fabrication cost of a die substantially drops as the die area is reduced [43], [85], MCMs can greatly reduce the total cost. With yield and technology scaling declining over chip fabrication generations, MCMs become one of the few left options for scaling systems. Recent Intel [72] and AMD [68], [69] CPUs are notable examples of MCMs; multiple chiplets containing several CPU cores and cache memory are integrated into a single package using EMIB [65] or CoWoS [39] packaging technologies. Also, numerous domain-specific architectures utilizing MCMs have been proposed [41], [63], [85], [88], [89]. In addition, MCM enables architects to adjust the granularity of a die depending on the area budget, ranging from AMD's high-end 74mm<sup>2</sup> die [69] to a more cost-effective 6mm<sup>2</sup> die of Simba [85].

These recent trends motivate us to design an MCM architecture for cost-effective FHE acceleration. By using MCMs, we can enjoy the aforementioned benefits coming from a significant reduction in individual die areas. Also, this approach is highly scalable because we can reuse the same design for each chiplet and place multiple chiplets to easily develop various MCM FHE accelerators with different computational throughput and bandwidth as required by the technology constraints and the purpose of use. Prior ASIC FHE accelerator proposals all include high bandwidth memories (HBMs), already assuming the use of advanced packaging for connecting HBMs to the chip. The same packaging can be utilized to connect multiple chiplets with little additional cost [53]. We utilize the open specification of Universal Chiplet Interconnect Express (UCIe) [91] to design and evaluate the MCM FHE accelerator.

<sup>1</sup>CraterLake refers to it as lane group.

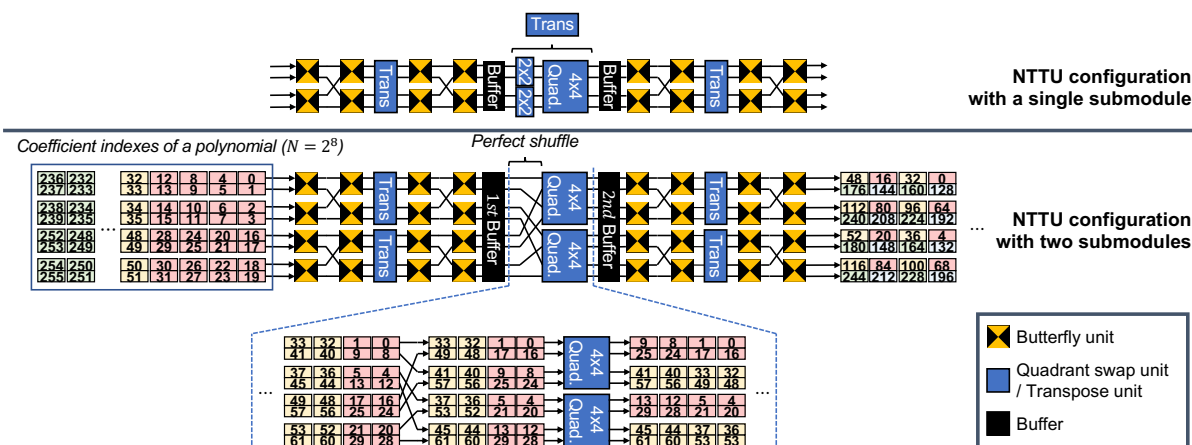


Figure 1: Exemplar configurations of a recomposable NTT unit, simplified to the  $N = 2^8$  case. A submodule, which is the smallest unit occupying  $\sqrt[4]{N}$  lanes, is shown above. A two-submodule configuration and its NTT process for a length- $N$  polynomial are shown below.

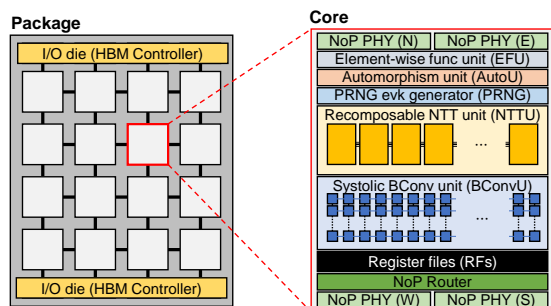


Figure 2: Organization of CiFHER. The CiFHER package is composed of multiple core chiplets and two I/O dies handling HBM. A core comprises several functional units (FUs), register files (RFs), and networking components.

### III. CiFHER MICROARCHITECTURE

To reduce the high cost of a monolithic chip design, we propose CiFHER, an MCM architecture for FHE acceleration. CiFHER has a tiled architecture with multiple chiplet *cores* connected by a mesh NoP. Fig. 2 depicts the package and core organization of CiFHER.

The main challenge in designing an MCM architecture lies in reducing the network on package (NoP) pressure. As deployable bandwidth and topology are heavily restricted by the technology constraints of the NoP, we devise novel data mapping methodologies (Section IV) and algorithms (Section V) addressing the high latency and low bandwidth of NoP. Nonetheless, prior to determining the configuration of the MCM package, we will first architect the internals of a chiplet core in this section.

#### A. Core Organization

Prior accelerators either utilize tiny (PE in BTS) or huge (cluster or lane group in F1, ARK, and CraterLake) cores, which do not provide much flexibility in design. In contrast, we design the cores of CiFHER to have varying computational throughput, which can be adjusted depending on the package

configuration. Based on the flexible design, we later identify the compelling combinations of the core design and the MCM package configuration.

A core comprises a *recomposable NTTU*, a *systolic BConv unit (BConvU)*, an *automorphism unit (AutoU)*, an *element-wise function unit (EFU)*, a *PRNG evk generator (PRNG)*, a router and PHYs for NoP communication, and register files (RFs). We adopt the vector architecture utilized in F1, CraterLake, and ARK, where we place multiple parallel lanes in a core. Each lane has a dedicated RF space not accessible by the other lanes, which enables maximizing parallelism with low costs for synchronization and arbitration. The vector architecture has shown effectiveness in reducing the communication overhead and the register file bandwidth pressure, which are major bottlenecks in FHE.

By combining effective components from different vector accelerators with proper modifications, CiFHER provides an enhanced representative core design for FHE accelerators. In particular, we adopt the distributed RF, systolic BConvU, and AutoU structures from ARK, and adopt PRNG from CraterLake. A systolic BConvU is composed of multiple multiply-accumulate (MAC) units, forming an output-stationary systolic array. We can adjust the configuration of a BConvU freely in a similar way to ARK, which uses a  $1 \times 6$  configuration per lane based on the design sweep of a BConvU. Moreover, most functional units (FUs) can be easily modified to support any power-of-two number of lanes in a vector core. However, the preceding vector NTTU, a critical component of a vector core, constitutes a substantial computing unit with 2,048 butterfly units and maintains a fixed organization (the number of lanes fixed to 256 in both ARK and CraterLake).

The inflexibility in previous large-scale NTTU designs imposes significant constraints on our design space, eventually leading to hardware inefficiency. Due to their lack of decomposability, previous designs require die areas large enough to contain bulky NTTUs. This makes it challenging to adjust the compute throughput of each core to balance computational

**Table I: Target parameters of CiFHER.**

Parameter Description	$N$ Degree	$L$ # of $q_i$	$K$ # of $p_i$	$Q$ $\prod_{i=1}^L q_i$	$P$ $\prod_{i=1}^K p_i$	Security (bits)
Value	$2^{16}$	$\leq 48$	12	$\leq 2^{1218}$	$2^{336}$	$\geq 128$ [11]

capability with the low NoP bandwidth, resulting in imbalanced and, thus, inefficient designs for an MCM.

### B. Recomposable NTT Unit

We devise a recomposable NTTU supporting various configurations with the number of lanes adjustable from 16 to 256. We regard a length- $N$  polynomial as a  $\sqrt{N} \times \sqrt{N}$  matrix, which allows us to perform 2D-FFT-style (i)NTT, performing  $\sqrt{N}$ -point (i)NTT along the rows and then along the columns in sequence. We then apply the four-step 2D FFT dataflow [9] to each of the row-direction and column-direction (i)NTTs. We obtain a compact NTTU spanning  $\sqrt[4]{N} = 16$  lanes shown in Fig. 1 (simplified to  $N = 2^8$ ), which we refer to as the *submodule* of our NTTU.

Up to 16 submodules can be stacked to deliver higher computational throughput for (i)NTT, providing flexibility for our design space exploration. We devise a method to combine multiple submodules to have them collaboratively perform (i)NTT on a limb by performing a perfect shuffle [87] between the submodules. The perfect shuffle enables the rearrangement of dispersed data across various submodules by transforming it into a sequence that can be effectively transposed using subsequent quadrant swap units. An exemplar two-submodule NTTU configuration for  $N = 2^8$  performing NTT is shown in Fig. 1. We regard a length- $2^8$  polynomial as a  $16 \times 16$  matrix. The first half of a submodule performs a four-step NTT on a row (data indices: 0–15/16–32). It starts from stride-1 butterfly ops and ends with stride-8 ops to perform 16-point NTT on a row. Then the buffering and shuffling steps in the middle redistribute the data between different submodules so that each submodule holds data elements with stride 16 in the second buffer; i.e., each submodule holds the elements of a column. Finally, the second half of a submodule performs a four-step NTT on a column (data indices: 0–240/4–244, stride 16) by starting from stride-16 butterfly ops and ending with stride-128 ops to perform 16-point NTT on a column.

Our recomposable NTTU also allows up to  $\sqrt[4]{N} = 16$  cores to perform (i)NTT of a limb together. In this case, data exchange between the collaborating cores occurs after the buffering and shuffling steps when performing NTT.

### C. Word Length & Logic Optimization

We choose 32 bits as the word length to use in CiFHER as it is beneficial to use short word lengths for the efficiency of logical operations. While BTS and ARK utilize a word length of 64 bits, which has been traditionally used in CKKS libraries [19], [26], [31], F1 (32 bits), CraterLake (28 bits), and FPGA FHE accelerators (FAB [1] (54 bits) and Poseidon [95] (32 bits)) utilize shorter word lengths. Despite using a relatively short word length, we maintain the high scale ( $\Delta$ ), and thus high

precision, by performing rescaling with two primes. When  $q_i \cdot q_{i+1} \simeq \Delta$  is satisfied, rescaling can be done by an approximate division by  $q_i \cdot q_{i+1}$  using RNS. We use high scales ranging from  $2^{47}$  to  $2^{55}$  for the evaluation in Section VI. Table I tabulates our target parameters.

We utilize the word-level Montgomery reduction circuit proposed in [66] with further enhancements using the signed Montgomery reduction algorithm in [83]. The circuit is utilized for all modular reduction circuits in CiFHER, including EFUs, NTTUs, PRNGs, and BConvUs.

**Systolic BConvU:** By using a 32-bit word length, more limbs are utilized (higher  $L$  and  $K$ ) than 64-bit ARK. Therefore, to provide higher word-level throughput for BConv, we use a longer  $1 \times 12$  BConv configuration per lane by default.

**EFU:** Inside an EFU, we place multiple modular multipliers, modular adders, and element-wise op circuits for specific purposes required in FHE (e.g., double-word accumulation and reduction). An EFU can perform compound element-wise ops to reduce the pressure on RFs.

## IV. DATA MAPPING METHODOLOGY

### A. Tiled Architecture

Due to the technology constraints of NoP, CiFHER necessarily becomes a tiled architecture connected by a mesh network. Due to the short channel reach of an advanced interface [91], a complex network topology that requires connections between distant nodes is unavailable for MCMs. Therefore, we fix the topology to 2D mesh as shown in Fig. 2. Also, due to the high cost of NoP communication, we set the default bisection bandwidth of the entire package to 2TB/s, which is several to an order of magnitude lower than that of CraterLake (29TB/s) or ARK (8TB/s).

Prior FHE accelerators co-design the data mapping method with the network on chip (NoC) organization. They design complex NoC structures using direct connections between distant nodes with high bandwidth and uniform communication time. However, in an MCM architecture with a mesh network, communication latency between nodes is non-uniform, as distant nodes are separated by multiple hops. Lagging data from distant nodes cause others to wait idly, degrading the overall performance [85]. The low bandwidth of NoP exacerbates this problem. Therefore, we delve into data mapping methodologies to reduce the pressure of the network.

### B. Combining Data Mapping Methods

Prior data mapping methods can be classified into *coefficient scattering* and *limb scattering*. Coefficient scattering is a method of distributing  $N$  coefficients of each limb equally to the entire computing units. By contrast, in limb scattering, each prime and the corresponding limbs are allocated to a specific computing unit. BTS and CraterLake use coefficient scattering, whereas F1 and ARK mostly use limb scattering. ARK temporarily switches to coefficient scattering during BConv, which we detail in Section V-A.

Due to the conflicting data access patterns of HE ops, core-to-core communication is inevitable regardless of the data

mapping method. (i)NTT and BConv, the two most dominant primitive functions, require different data mapping due to their data access patterns. For a polynomial, which is expressed as an  $\ell \times N$  matrix, (i)NTT can be separately applied to each of  $\ell$  limbs, making limb scattering a favorable option. By contrast, as BConv is mostly a matrix-matrix mult with a  $K \times \ell$  BConv table (see Section II-C), data access is performed along the columns of a polynomial and makes coefficient scattering a better option. Therefore, data exchange between cores is required either during (i)NTT (coefficient scattering) or BConv (limb scattering).

In an accelerator with many cores, both data mapping methods have limitations. As the rescaling makes the number of limbs ( $\ell$ ) vary over HE ops, it is difficult to distribute the limbs equally to cores without causing *fragmentation* issues in limb scattering. A core will be assigned fewer limbs than others depending on  $\ell$  and wait idly for others to finish processing. In contrast, coefficient scattering is free from fragmentation issues because the degree of a polynomial ( $N$ ) does not change. However, coefficient scattering has a scaling limit due to quadratic growth in the number of transferred packets with increasing cores. For example, during (i)NTT, all-to-all data exchange between the cores is required when using coefficient scattering. When  $k$  number of cores are participating in coefficient scattering, each core should send  $k - 1$  packets, requiring a total of  $k^2 - k$  packets to be transferred. These issues become more severe as more cores participate in the distribution. Also, with more cores, additional performance degradation from long *tail latency* in lagging data occurs.

Therefore, in an MCM architecture with many cores and restrained NoP bandwidth, the combined use of limb scattering and coefficient scattering enhances performance, even with the increased total amount of transferred data due to performing data exchanges for both (i)NTT and BConv. We partition a polynomial in both limb and coefficient directions by dividing cores into *limb clusters* and *coefficient clusters*. A limb cluster is a set of cores each holding an evenly distributed subset of the coefficients of a limb. By contrast, the cores in a coefficient cluster partition the residues of a coefficient corresponding to different primes. Then, (i)NTT or BConv only incurs data exchange within each limb cluster or coefficient cluster, reducing the number of cores participating in the exchange. Therefore, combining two data mapping methods suffers less from the aforementioned issues, leading to performance enhancement.

### C. Generalized Data Mapping Methods for a Tiled FHE Accelerator

We introduce two generalized data mapping methods that combine coefficient scattering and limb scattering for mapping HE ops to a tiled architecture: *dimension-wise clustering* and *block clustering*. Determining the data mapping method is equivalent to a problem of determining how to compose limb clusters and coefficient clusters.

Dimension-wise clustering binds the cores on the same vertical line into a limb cluster and the cores on the same

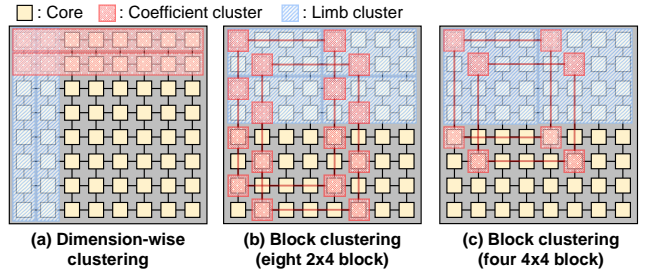


**Figure 3: Generalized data mapping methods of CiFHER with 64 cores: (a) dimension-wise clustering and block clustering for two different exemplar block sizes of (b)  $2 \times 4$  and (c)  $4 \times 4$ .**

horizontal line into a coefficient cluster, or in the opposite directions, on a mesh network. Fig. 3a shows an example of dimension-wise clustering on an  $8 \times 8$  mesh. This distribution method has the advantage that each data exchange process of (i)NTT and BConv can be performed without interference because data movement occurs in different axial directions. However, the configuration is fixed for a given mesh shape, potentially sharing the same limitations of prior mapping methods when the mesh shape is skewed.

Block clustering is a more generalized mapping method than dimension-wise clustering. Block clustering places limb clusters in the form of blocks with an arbitrary size, and forms coefficient clusters with cores in the same position within each block. Fig. 3b and Fig. 3c show exemplar configurations dividing an  $8 \times 8$  mesh into eight  $2 \times 4$  or four  $4 \times 4$  limb cluster blocks. Unlike dimension-wise clustering, various block clustering configurations are possible by changing the size of a block. We refer to the configuration on a  $d_x \times d_y$  mesh using a  $b_h \times b_w$  block size as  $d_x \times d_y$ -BK- $b_h \times b_w$ . Dimension-wise clustering is simply denoted as  $d_x \times d_y$ -DW, which is indeed a special variant of block clustering; e.g., Fig. 3a can be expressed as  $8 \times 8$ -BK- $8 \times 1$ . Also, limb scattering and coefficient scattering can be expressed as  $d_x \times d_y$ -BK- $1 \times 1$  and  $d_x \times d_y$ -BK- $d_x \times d_y$ , respectively.

Maximizing the performance of CiFHER requires to consider various factors as the data mapping method has conflicting effects on performance. In addition to the trade-offs discussed in Section IV-B, our generalized data mapping methods reduce the maximum number of hops packets travel by restricting their movement within a cluster composed of adjacent cores. Also, the balance between limb clusters and coefficient clusters is important in our methods because an unbalanced configuration would result in fragmentation issues and/or severe performance degradation as either (i)NTT or BConv ops must wait for the other to finish due to the dependency in common CKKS use cases. We discover the best configuration in Section VI through an extensive simulation that accounts for all these factors.

## V. ALGORITHMIC OPTIMIZATIONS

### A. Limb Duplication for BConv

We propose a novel *limb duplication* algorithm, which duplicates the input limbs of BConv to reduce the amount

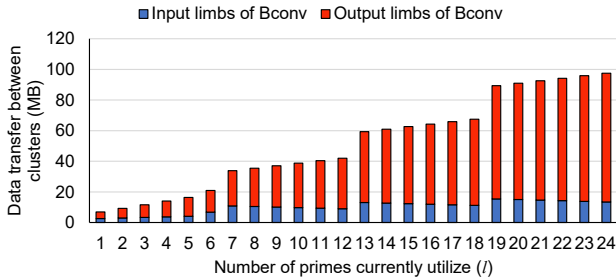


Figure 4: The amount of data transfer during key-switching using the method of ARK [54] under different  $\ell$  conditions.

of data communication caused by the redistribution of the output limbs during BConv. Limb duplication is effective when the residues of a coefficient are distributed across multiple cores in a coefficient cluster.

BConv in key-switching requires gathering the residues from different cores. F1 utilizes parameters that allow it to perform BConv for each of the  $\ell$  limbs in parallel without redistribution of input data ( $\ell$  limbs) before BConv [19]. However, the BConv part of F1 produces massive  $\ell^2$  output limbs, which need to be redistributed among cores. More recently proposed ARK adopts a parameter choice that makes BConv produce fewer limbs (roughly  $\ell \cdot \beta$  limbs for a small integer  $\beta$ ), which also significantly reduces the amount of computation [36]. However, as it becomes harder to parallelize BConv, ARK switches to coefficient scattering prior to BConv and switches back to limb scattering after BConv, inducing data redistribution of both input and output data of BConv. Fig. 4 shows the estimated amount of data transfer required for key-switching depending on  $\ell$  (the number of primes) when using ARK’s method. Because the number of input limbs is usually smaller than the number of output limbs, the output limbs of BConv account for most of the data transfer regardless of  $\ell$ .

To eliminate the data transfer required for the redistribution of generated limbs, limb duplication duplicates input limbs and broadcasts them to all the cores in a coefficient cluster so that each core holds the entire polynomial ( $\ell \times N$  matrix when only considering limb scattering). Then, each core performs BConv with a piece of the BConv table ( $K \times \ell$  matrix). For example, if a core is in charge of the primes  $p_1, p_5$ , and  $p_9$ , it will only multiply the 1<sup>st</sup>, 5<sup>th</sup>, and 9<sup>th</sup> rows of the BConv table with the polynomial to obtain BConv results. As the output limbs already belong to the right owner, data redistribution after BConv is unnecessary.

However, limb duplication requires additional data transfer for broadcasting input limbs. The overhead of broadcasting varies depending on the ratio of the number of input limbs and the number of output limbs and the data mapping methodology. We can formulate the reduction in the number of transferred limbs compared to the ARK’s method as in Eq. 3.  $\text{broadcast}_{\text{overhead}}$  denotes the ratio of data transfer required for broadcasting compared to that required for even distribution

and has a value greater than one.

$$\#\text{limbs}_{\text{output}} - \#\text{limbs}_{\text{input}} \times (\text{broadcast}_{\text{overhead}} - 1) \quad (3)$$

Eq. 3 must be larger than zero to make limb duplication beneficial. We selectively use limb duplication only when this condition is satisfied for each BConv. As there are much more output limbs than input limbs as shown in Fig. 4, limb duplication is usually beneficial for the reduction of communication between cores.

### B. An Eclectic Approach to Prior Algorithms

We adopt the state-of-the-art CKKS algorithms mostly from an FHE CPU library, Lattigo [31]. We combine the bootstrapping algorithms from [12], [18]. There are also accelerator-specific algorithms. For example, ARK proposes two algorithms, *minimum key-switching* and *on-the-fly limb extension*, which result in substantial reductions in the off-chip memory access, solving the bandwidth bottleneck from which prior accelerators suffered [57], [82]. We explain how such algorithms can (or cannot) be applied to CiFHER.

**Minimum key-switching:** The loading time of evks becomes a critical bottleneck in accelerators as each evk can be as large as several MBs. Most of the evks are for HRot ops, which require a different  $\text{evk}_r$  for each rotation amount ( $r$ ). ARK builds on the algorithm proposed in [34] to suggest the minimum key-switching algorithm for HRot ops. The algorithm targets HRot ops with rotation amounts forming an arithmetic progression, which are common computational patterns found in CKKS, and performs HRot ops recursively by a rotation amount equal to the common difference of the progression. By applying the algorithm, only one  $\text{evk}_r$  is required for a sequence of HRot ops. As reducing the off-chip memory access for evks is also crucial in CiFHER, we adopt minimum key-switching in CiFHER.

**On-the-fly limb extension:** Plaintexts (polynomials) required for PMult ops also account for a considerable portion of off-chip memory access. For example, a bootstrapping op requires several GBs of plaintexts. On-the-fly limb extension compresses each plaintext to occupy only one limb per polynomial and generates the rest at runtime. However, the runtime extension involves performing NTT, incurring expensive NoP data transfer. As the overall cost for runtime extension exceeds the benefits coming from the reduced off-chip memory access in an MCM architecture, we do not use this algorithm in CiFHER.

**PRNG evk generation:** We adopt the PRNG evk generation from CraterLake. The  $\mathbf{a}$  parts of evks are purely random polynomials. Therefore, by deploying deterministic PRNG circuits inside a chip, they can be generated on-the-fly using a short seed, reducing the off-chip memory access for evks to half [82]. As evks can be generated within each core in parallel, no additional overhead is required for MCMs.

## VI. EVALUATION

### A. Implementation & Default Configurations

**Performance modeling:** To evaluate the performance of CiFHER, we implemented a cycle-accurate simulator for a

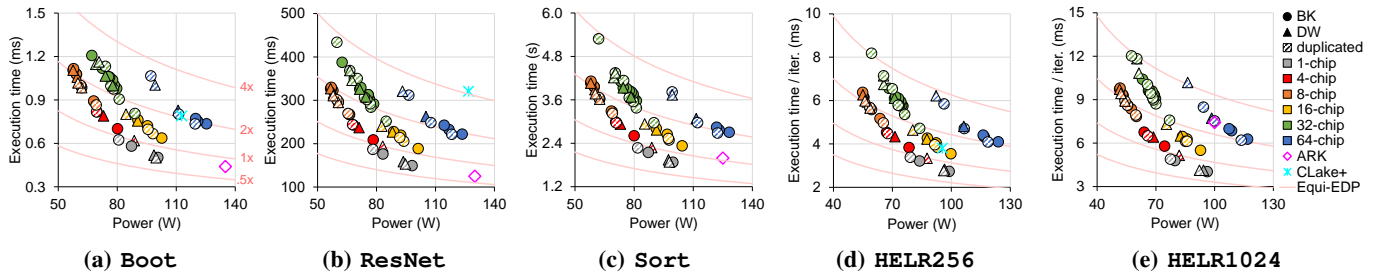


**Figure 5: Performance comparison between CiFHER default configurations and prior vector FHE accelerators, (a)(b)(d) CLake+ and (a)(b)(c)(e) ARK, for the workloads.  $n$ -chip denotes the default configuration of CiFHER with  $n$  core chiplets, except for 1-chip, which is modified from 4-chip to integrate 4 cores into a monolithic die and has double bisection bandwidth to account for the bandwidth gap between NoC and NoP. BK: block clustering, DW: dimension-wise clustering, duplicated: using limb duplication.**

**Table II: Area breakdown of the default configurations of CiFHER with varying numbers of cores.**

Configuration	Area / core (mm <sup>2</sup> )				
	4 core (2 × 2)	8 core (2 × 4)	16 core (4 × 4)	32 core (4 × 8)	64 core (8 × 8)
Register files	31.71	15.86	7.93	3.96	1.98
NTTU	3.75	1.82	0.88	0.43	0.22
BConvU	1.07	0.65	0.44	0.34	0.28
EFU	0.72	0.36	0.18	0.09	0.05
AutoU	2.32	0.58	0.14	0.04	0.01
PRNG	0.71	0.36	0.18	0.09	0.04
Router/PHY	6.80	3.40	3.40	1.70	1.70
Total	47.08	23.02	13.15	6.65	4.28
Configuration	Package area (mm <sup>2</sup> )				
	4 core (2 × 2)	8 core (2 × 4)	16 core (4 × 4)	32 core (4 × 8)	64 core (8 × 8)
Cores	188.32	184.13	210.43	212.75	273.87
I/O dies	36.71				
Total	225.04	220.84	247.14	249.46	310.59

multi-core system. We implemented various core and package organizations, data mapping methods, and algorithms on the simulator, which allows us to explore a vast design space to discover compelling combinations. The simulator takes a sequence of HE ops as input and translates it into a flow graph of instructions. It divides instructions into micro-instructions and maps the micro-instructions to chiplets according to the data mapping method. The simulator tracks the status of data transmission, data dependency between micro-instructions, and virtual channel allocation status of the NoP to avoid structural hazards and functionality issues. Micro-instructions are scheduled based on this tracking data. Our simulator adopts the decoupled data orchestration of CraterLake to prefetch data from HBM using the static nature of HE ops.

**Hardware modeling:** We synthesized major logic components in RTL using the ASAP7 7.5-track 7nm process design kit (PDK) [24]. Large SRAM components with a bank size larger than 2KB were evaluated using a memory modeling tool, FinCACTI [84]. We extensively modified FinCACTI to match the IEEE IRDS roadmap [42], ASAP7, and other published data in 7nm technology nodes [17], [47], [49], [71], [86], [93]. We used published data for HBM [74] and PHYs [49], [91]. We integrated the results into the performance modeling tool to automatically derive power and die area. Overhead due to

long wires is also estimated in the tool. All components run at 1GHz.

**Routing and NoP implementation:** We used XY routing and  $5 \times 5$  virtual channel routers [29] for NoP communication, which is a simple yet effective solution for the highly balanced traffic pattern of CiFHER. Each input and output port has 4 virtual channels. We modeled NoP performance and energy using the specification of the UCIe advanced package with a PHY supporting 16GT/s of transfer rate [91].

**Memory instances:** Two types of RFs, the main *scratchpad RF* and an *auxiliary RF* for key-switching, are utilized in CiFHER. The RFs together can provide 6 reads and 6 writes per lane in a cycle through bank interleaving [73]. We modeled the NoP traffic for HBM access by injecting packets through edges connecting the I/O die and its adjacent cores on our simulator. The bandwidth of this edge is the same as that of edges connecting the cores. Two HBM stacks are utilized, each providing 500GB/s of bandwidth [45], [46].

**CiFHER default configurations:** The default configurations are the ones with different numbers of cores but having similar levels of total computational throughput and memory bandwidth. Due to the use of the recomposable NTTUs, we can adjust the number of vector lanes in a core from 16 to 256. We fixed  $(\# \text{ of cores}) \times (\# \text{ of lanes in a core})$  to 1,024 to make different configurations have a similar level of total computational throughput. Also, we fixed the bisection bandwidth and the aggregate RF capacity of the package. We fixed the bisection bandwidth of the package to 2TB/s and decided the bandwidth of each edge by dividing it by the number of edges crossing the bisection. The aggregate capacity of auxiliary RFs was set to 16MB (e.g., 1MB per core in a 16-core configuration). Also, we used a total of 256MB of scratchpad RF space, which we found to be sufficient for CiFHER when using PRNGs and is the same as the RF capacity of CraterLake. Table. II shows the area breakdown of the default configurations of CiFHER.

## B. Experimental Setup

We simulated the performance and power consumption of various configurations of CiFHER. We utilized four representative workloads that are the most sophisticated FHE



workloads currently available and that have also been utilized for evaluating the previous accelerators.

**CKKS bootstrapping (Boot):** FHE CKKS workloads require frequent bootstrapping, each of which involves hundreds of primitive HE ops. Therefore, bootstrapping accounts for most of the execution time in representative workloads [54]. We performed CKKS bootstrapping of a ciphertext containing  $2^{15}$  complex numbers. We divided the execution time with the number of rescaling ops possible in between consecutive bootstrapping ops (nine in our parameters with  $L = 48$ ) to account for the frequency of bootstrapping.

**CNN inference (ResNet):** We used a CKKS implementation [60] of the ResNet-20 model for CIFAR-10. We report the latency of a single-image inference, which takes 2,271 seconds in the original single-threaded CPU implementation.

**Sorting  $2^{14}$  numbers (Sort):** We used the two-way sorting implementation from [38]. The original 32-thread CPU implementation takes 23,066 seconds to finish.

**Logistic regression training (HELR):** We used the implementation from [35]. We performed encrypted training with a binary classification model for classifying the numbers 3 and 8 in the MNIST dataset. We performed 32 iterations of single-batch training and report the average execution time per iteration. We tested for two batch sizes of 256 (HELR256) and 1,024 (HELR1024).

We compared performance and efficiency with CraterLake and ARK using their reported performance and power values under 128-bit security constraints. For 12/14nm CraterLake, optimistic compensations for the difference in the technology node (14nm to 7nm [71]) were applied to its chip area and power, which we denote CLake+.

### C. Performance & Efficiency

Fig. 5 shows the performance and power consumption of CiFHER default configurations using various data mapping methods and algorithms. We limited the number of limb clusters to eight to avoid severe fragmentation issues. Among the default configurations, 4-core CiFHER using dimension-wise clustering and limb duplication showed the best energy-delay product (EDP), whose values are shown with the  $1\times$  equi-EDP lines in Fig. 5. When we integrated the 4 cores into a single monolithic die and connected the cores in the NoC with  $2\times$  higher bisection bandwidth (1-chip in Fig. 5), additional performance and EDP enhancements were achieved. However, 1-chip CiFHER’s fabrication cost would be as prohibitively high as prior accelerators due to the large chip area. 1-chip CiFHER resembles ARK with datapath reduced to 32 bits and showed a similar EDP with the original 64-bit ARK except for HELR1024. The reason for ARK’s relative performance degradation in HELR1024 is that we reordered the HE ops to further enhance the reuse of evks in the memory-bound region, which ARK identifies as a bottleneck of HELR.

As we split the chip and utilize smaller cores, performance and efficiency inevitably decline because more NoP data transfer is required. Therefore, the area constraint is a decisive factor in an MCM FHE accelerator design. If the cost budget allows,

**Table III: Execution time and relative energy-delay-area product (EDAP) [62] of CiFHER and prior vector FHE accelerators.**

Execution time (ms), the lower the better					
	CLake+	ARK	CiFHER 4 cores	16 cores	64 cores
Boot	0.79	<b>0.44</b>	0.62	0.64	0.73
ResNet	321	<b>125</b>	194	189	222
Sort	-	<b>1990</b>	2282	2328	2683
HELR256	3.81	-	<b>3.34</b>	3.55	4.09
HELR1024	-	7.42	<b>5.16</b>	5.50	6.20
Relative EDAP (vs. 4-core CiFHER), the lower the better					
Boot	2.04 $\times$	1.46 $\times$	1.00 $\times$	1.35 $\times$	2.63 $\times$
ResNet	4.09 $\times$	1.20 $\times$	1.00 $\times$	1.26 $\times$	2.56 $\times$
Sort	-	2.04 $\times$	1.00 $\times$	1.34 $\times$	2.62 $\times$
HELR256	1.40 $\times$	-	1.00 $\times$	1.41 $\times$	2.80 $\times$
HELR1024	-	4.70 $\times$	1.00 $\times$	1.42 $\times$	2.77 $\times$

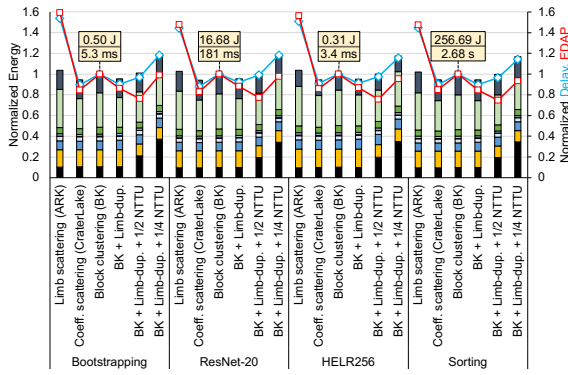
as in recent AMD server CPUs (74mm<sup>2</sup> per compute die [69]), utilizing four cores would be the best option. Table III shows that 4-core CiFHER achieves enhanced efficiency in terms of energy-delay-area product (EDAP) [62] with comparable performance to prior monolithic FHE accelerators due to significantly lower power dissipation (see Fig. 5). Compared to ARK, 4-core CiFHER performs 1.15 $\times$  slower but reduces the EDAP by 2.03 $\times$  in geometric mean (geomean) of the workloads. Compared to CLake+, it performs 1.34 $\times$  faster and results in a 2.27 $\times$  EDAP reduction. On the other hand, if we can only afford dies as small as recent domain-specific MCM accelerator proposals, such as NN-Baton [89] (2mm<sup>2</sup>) and Simba [85] (6mm<sup>2</sup>), 16-core or 64-core CiFHER needs to be utilized.

Nevertheless, our data mapping methods and limb duplication minimize the performance and efficiency degradation of many-core configurations. The best 16-core and 64-core configurations respectively perform only 1.03 $\times$  and 1.18 $\times$  slower in geomean than 4-core. Compared to 4-core, EDP increases to 1.23 $\times$  (16-core) and 1.94 $\times$  (64 core), and EDAP increases to 1.35 $\times$  (16-core) and 2.67 $\times$  (64-core) in geomean using our optimized configurations, whereas a naïve configuration (e.g., 64-core using limb scattering with ARK’s method) would require 17.1 $\times$  higher EDP and 23.6 $\times$  higher EDAP in bootstrapping. We will analyze the contributions of each factor thoroughly in the following sections.

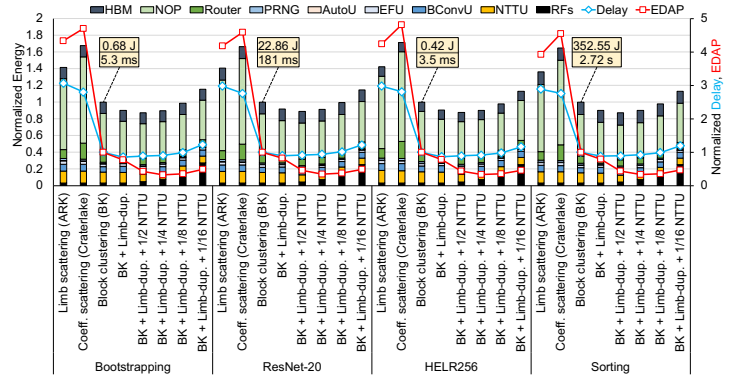
Meanwhile, due to the skewed organization, 8-core ( $2\times 4$ ) and 32-core ( $4\times 8$ ) configurations suffer from an imbalance in NoP throughput between the horizontal and vertical directions, increasing the tail latency. As a result, performance drops severely, making these configurations less attractive.

### D. Sensitivity Study

To comprehensively evaluate the effects of our data mapping, algorithmic optimization, and core microarchitecture in many-core configurations, we estimated energy, delay, and EDAP of CiFHER while incrementally adopting block clustering ( $4\times 4$ -BK- $2\times 2$  and  $8\times 8$ -BK- $4\times 4$ ), limb duplication, and recomposable NTTUs. Fig. 6 displays the results.



(a)  $4 \times 4$  configuration



(b)  $8 \times 8$  configuration

**Figure 6: Delay, energy breakdown, and energy-delay-area product (EDAP) [62] of CiFHER when incrementally applying our block clustering (BK) data mapping, limb duplication (Limb-dup.), and reducing the number of lanes in a core using the recomposable NTTU. For our data mapping,  $4 \times 4$ -BK- $2 \times 2$  and  $8 \times 8$ -BK- $4 \times 4$  were used.**

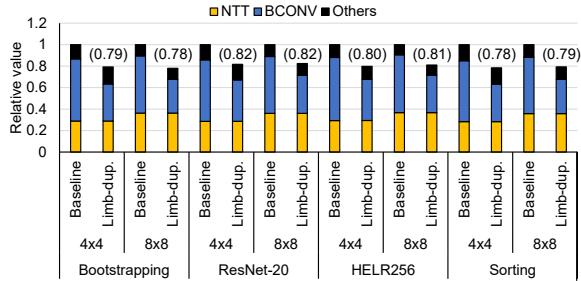


**Figure 7: Amount of data movement between cores as CiFHER performs each workload with and without limb duplication. Baseline corresponds to ‘Block clustering (BK)’ in Fig. 6 and Limb-dup. to ‘BK + Limb-dup.’ in Fig. 6.**

Limb scattering resulted in  $1.44$ – $1.53 \times$  ( $4 \times 4$ ) and  $2.89$ – $3.06 \times$  ( $8 \times 8$ ) slowdowns compared to our block clustering method. Coefficient scattering was  $1.10$ – $1.13 \times$  faster than our method for the  $4 \times 4$  configuration, whereas it was  $2.76$ – $2.81 \times$  slower for  $8 \times 8$ . The data exchange pattern when using limb scattering is not all-to-all as we can group some limbs together to have data transfer occur within each group. In contrast, coefficient scattering requires all-to-all data exchange and thus scales poorly for a large number of cores than limb scattering. Coefficient scattering consumes  $2.07 \times$  more energy on NoP and shows  $4.66 \times$  higher (worse) EDAP than our mapping in geomean for the  $8 \times 8$  configuration. Yet, all-to-all data exchange between 16 cores is manageable, making coefficient scattering faster than our mapping for  $4 \times 4$ .

The use of limb duplication leads to solid delay and energy reductions. Fig. 7 compares the amounts of data movement between the cores of CiFHER for each workload, with and without limb duplication. For all circumstances, limb duplication eliminated 18–22% of the data movement between the cores. When limb duplication was applied to our mapping in the  $4 \times 4$  configuration, we obtained  $1.10 \times$  delay and  $1.16 \times$  EDAP reductions in geomean, and the delay and EDAP gaps

with coefficient scattering were also reduced to only 1.3% and 2.1% in geomean.

Finally, recomposable NTTUs increase the hardware efficiency of CiFHER by enabling a compact MCM architecture with a balance between computational throughput and available data movement bandwidth. We reduced the number of lanes in a core from 256 (16 NTTU submodules) to  $1/2$ ,  $1/4$  (default configuration for  $4 \times 4$ ),  $1/8$ , and  $1/16$  (default configuration for  $8 \times 8$ ) of 256 by using our recomposable NTTUs. In the  $4 \times 4$  configuration, the optimal EDAP was achieved with  $1/2$  NTTU (equivalent to eight NTTU submodules), while it was achieved with  $1/4$  NTTU (four NTTU submodules) in the  $8 \times 8$  configuration.  $1/2$  NTTU resulted in a minimal 7% performance degradation and a  $1.14 \times$  EDAP enhancement in geomean for the  $4 \times 4$  configuration (vs. BK + Limb-dup.).  $1/4$  NTTU resulted in a minimal 5% performance degradation and a  $2.36 \times$  EDAP enhancement in geomean for the  $8 \times 8$  configuration (vs. BK + Limb-dup.).

### E. Limb Duplication Effects

The effects of limb duplication differ by each configuration. We selected the three best-performing configurations for each number of cores in Fig. 5a and compared the performance of bootstrapping with and without applying limb duplication. Fig. 8a shows the results. Limb duplication improved bootstrapping performance by up to 31% for  $4 \times 8$ -BK- $4 \times 4$  but rather caused 28% performance degradation for  $8 \times 8$ -BK- $2 \times 4$ .

Although limb duplication reduces the total amount of limbs exchanged, the bursty data transfer characteristic of broadcasting causes network contention and introduces additional latency. The overhead of broadcasting in limb duplication is affected by the arrangement of limb clusters.  $8 \times 8$ -BK- $2 \times 4$  is the only configuration in Fig. 8a with a coefficient cluster composed of eight cores; coefficient clusters in the other configurations are composed of one to four cores. The large number of cores in a coefficient cluster greatly increases the broadcasting latency, resulting in the performance degradation observed.

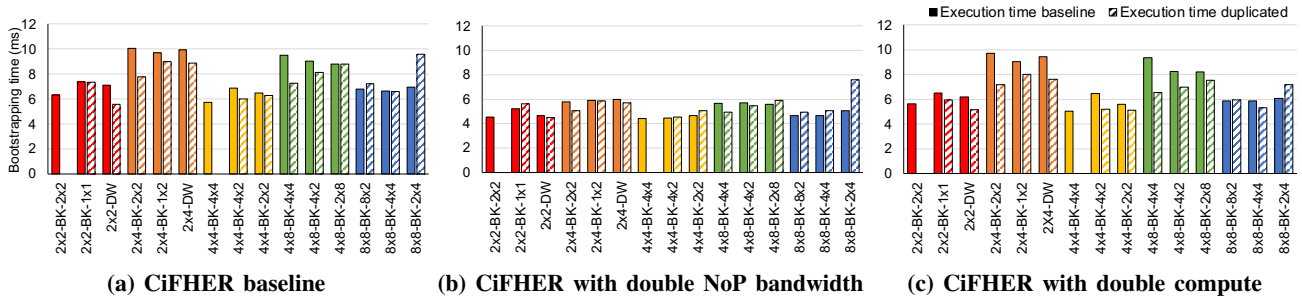


Figure 8: Bootstrapping performance of CiFHER with and without limb duplication. The three best-performing mapping configurations were selected for each number of cores. ARK’s redistribution method for BConv was used when limb duplication was not used.

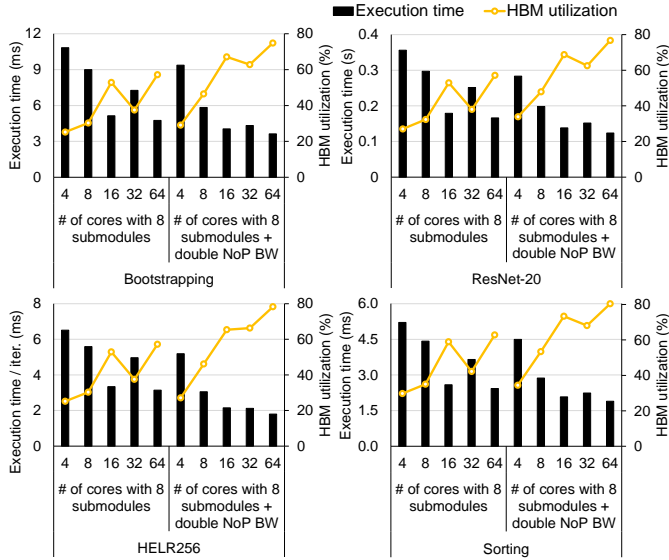


Figure 9: Performance of CiFHER while scaling the number of cores under default and double NoP bandwidth conditions. The number of NTT submodules in each core is fixed to eight.

As limb duplication is effective for reducing the NoP pressure, increasing the NoP bandwidth reduced the performance gains from using limb duplication (see Fig. 8b). Limb duplication enhanced the performance of the baseline configurations by 7% in geomean. With the NoP bandwidth doubled, limb duplication rather decreased performance by 3% in geomean, and the maximum performance gain observed for 4x8-BK-4x4 was reduced to 14% from 31% in the baseline.

Conversely, when we made the NoP bandwidth bottleneck more significant by doubling the computational throughput, performance gains from using limb duplication increased (see Fig. 8c). In these configurations, limb duplication enhanced performance by 14% in geomean, and the maximum performance gain reached 43%.

#### F. Scalability

To evaluate the scalability of CiFHER, we estimated the performance of each workload while increasing the number of cores and report it in Fig. 9. In the experiments, we set the internals of a core fixed to an eight-NTTU-submodule setting (128 lanes). Limb duplication and  $d_x \times d_y$ -BK- $d_x/2 \times d_y/2$  block clustering were used for a  $d_x \times d_y$  package configuration.

We set the HBM bandwidth and the bisection bandwidth of a package fixed. Therefore, the bandwidth of a network edge decreases as the number of cores increases.

The limited bandwidth of NoP restricts the scalability of CiFHER. When we increased the number of cores from 4 to 16,  $1.99\text{--}2.11\times$  of speedups were achieved for the workloads. Increasing from 16 to 64 only resulted in a  $1.07\times$  speedup in geomean. Therefore, increasing the number of cores without consideration for proper sizing of the core has an adversarial effect on efficiency. Meanwhile, skewed configurations (8-core and 32-core) showed suboptimal performance.

HBM bandwidth becomes the next limiting factor for scalability when NoP bandwidth is sufficient. Doubling NoP bandwidth mitigates the NoP pressure and improves the performance of the 16-core configuration by  $1.34\times$  in geomean. Also, scalability slightly improves as 4-to-16 and 16-to-64 number-of-cores transitions result in  $2.23\times$  and  $1.13\times$  speedups. However, the degree of speedups still falls largely behind the increase in the number of cores as the hardware becomes bottlenecked by the HBM bandwidth, whose utilization reaches 75–80% in the 64-core configuration.

## VII. RELATED WORK

**Function-level acceleration and leveled HE (LHE):** [51] accelerates non-RNS CKKS using Intel AVX-512 instructions and GPUs. HEXL [10] specifically utilizes AVX512-IFMA52 instructions for further CPU optimization. Also, to exploit the high degree of parallelism in major functions, many studies have attempted GPU acceleration. [97] accelerates (i)NTT through high-radix FFT and instruction-level optimizations. [56] identifies off-chip memory access as the performance bottleneck of (i)NTT on GPUs and applies a better use of the memory hierarchy of GPUs, improving data reusability to address the bottleneck. [5] accelerates the BFV [3], [15] scheme by replacing the major functions with ones more suitable for GPUs. [4] further partitions data to multiple GPUs to exploit abundant parallelism inside BFV.

Also, numerous FPGA work has attempted to optimize core HE ops by deploying tailored datapaths. [80] and [90] propose FPGA coprocessors with specialized FUs for the BFV scheme. HEAX [79] and coxHE [37] design FPGA modules targeting key-switching, a dominant HE op in CKKS. [58] supports

larger parameters adequate for FHE CKKS; however, it only accelerates (i)NTT.

Meanwhile, to overcome the limitations of LHE, Cheeta [76] (ASIC) and FxHENN [98] (FPGA) propose accelerators for the combined use of LHE with multi-party computation (MPC) for CNN inference. SRAM-based computing-in-memory architecture has also been proposed [78]. Despite not fully supporting FHE, these acceleration results can partially be extended to FHE; e.g., HEXL is currently adopted in CPU FHE libraries [2], [19].

**Torus LWE (TLWE) FHE:** TLWE-based FHE schemes [22], [30] are fundamentally different from RLWE in that usually a single prime modulus (single limb) is utilized. Many recent studies have specifically targeted the TFHE [22] scheme. cuFHE [92] speeds up TFHE computations on a GPU by utilizing primitive functions accelerated in cuHE [28], which uses a specialized prime to reduce the cost of modular reduction. [70] implements an FPGA datapath for an optimized TFHE bootstrapping algorithm using inter-operation parallelism. Meanwhile, in TFHE, floating-point Fourier transform is often used instead of NTT. [67] utilizes bit-level parallelism and the NVIDIA cuFFT library to accelerate TFHE on CPUs and GPUs. Matcha [48] is the first ASIC proposal and devises an approximate integer FFT method that replaces mult ops with shift and add ops.

**Ring LWE (RLWE) FHE:** [50] applies kernel fusion and parameter optimization to accelerate CKKS bootstrapping on GPUs. TensorFHE [33] utilizes the tensor cores in recent NVIDIA GPUs for (i)NTT. FAB [1] focuses on reducing the working set to alleviate the off-chip memory bandwidth bottleneck even with limited FPGA memory space. Poseidon [95] builds a 512-lane vector FPGA architecture with FUs reducing the on-chip memory bandwidth pressure, such as high-radix NTTUs. GPU and FPGA solutions achieve orders of magnitude higher performance compared to CPU but recent ASIC FHE accelerators [54], [57], [81], [82] introduced in Section II-D achieve even higher performance gains.

## VIII. CONCLUSION

In this paper, we have proposed CiFHER, a fully homomorphic encryption (FHE) accelerator based on a multi-chip module (MCM). We have devised methods for minimizing die-to-die communication, which incurs serious latency and energy overhead for an MCM. Our generalized data mapping methods limit the data communication to happen within a cluster, reducing the traveling distance of data and alleviating the network pressure. Also, a novel limb duplication algorithm eliminates data transfer caused by the redistribution of output data during base conversion, a key function of FHE. By utilizing multiple chiplets having a resizable structure, which is enabled by the use of recomposable number-theoretic transform units (NTTUs), we have created various optimized MCM package configurations of CiFHER. Multiple chiplets, each of which can be configured to be as small as  $4.28\text{mm}^2$ , collaborate efficiently with our data mapping methods and algorithms; the resulting

CiFHER package achieves comparable performance to state-of-the-art monolithic ASIC FHE accelerators with significantly reduced area and energy.

## REFERENCES

- [1] R. Agrawal, L. de Castro, G. Yang, C. Juvekar, R. Yazicigil, A. Chandrakasan, V. Vaikuntanathan, and A. Joshi, "FAB: An FPGA-based Accelerator for Bootstrappable Fully Homomorphic Encryption," in *HPCA*, 2023, pp. 882–895.
- [2] A. Al Badawi, J. Bates, F. Bergamaschi, D. B. Cousins, S. Erabelli, N. Genise, S. Halevi, H. Hunt, A. Kim, Y. Lee, Z. Liu, D. Micciancio, I. Quah, Y. Polyakov, S. R.V., K. Rohloff, J. Saylor, D. Suponitsky, M. Triplett, V. Vaikuntanathan, and V. Zucca, "OpenFHE: Open-Source Fully Homomorphic Encryption Library," in *Workshop on Encrypted Computing & Applied Homomorphic Cryptography*, 2022, pp. 53–63.
- [3] A. Al Badawi, Y. Polyakov, K. M. M. Aung, B. Veeravalli, and K. Rohloff, "Implementation and Performance Evaluation of RNS Variants of the BFV Homomorphic Encryption Scheme," *IEEE Transactions on Emerging Topics in Computing*, vol. 9, no. 2, pp. 941–956, 2019.
- [4] A. Al Badawi, B. Veeravalli, J. Lin, N. Xiao, M. Kazuaki, and A. Khin Mi Mi, "Multi-GPU Design and Performance Evaluation of Homomorphic Encryption on GPU Clusters," *IEEE Transactions on Parallel and Distributed Systems*, vol. 32, no. 2, pp. 379–391, 2021.
- [5] A. Al Badawi, B. Veeravalli, C. F. Mun, and K. M. M. Aung, "High-performance FV Somewhat Homomorphic Encryption on GPUs: An Implementation using CUDA," *IACR Transactions on Cryptographic Hardware and Embedded Systems*, pp. 70–95, 2018.
- [6] M. Albrecht, M. Chase, H. Chen, J. Ding, S. Goldwasser, S. Gorbunov, S. Halevi, J. Hoffstein, K. Laine, K. Lauter, S. Lokam, D. Micciancio, D. Moody, T. Morrison, A. Sahai, and V. Vaikuntanathan, "Homomorphic Encryption Standard," in *Protecting Privacy through Homomorphic Encryption*. Springer, 2021, pp. 31–62.
- [7] A. Arunkumar, E. Bolotin, B. Cho, U. Milic, E. Ebrahimi, O. Villa, A. Jaleel, C.-J. Wu, and D. Nellans, "MCM-GPU: Multi-Chip-Module GPUs for Continued Performance Scalability," in *ISCA*, 2017, pp. 320–332.
- [8] A. A. Badawi and Y. Polyakov, "Demystifying Bootstrapping in Fully Homomorphic Encryption," *Cryptology ePrint Archive*, Paper 2023/149, 2023. [Online]. Available: <https://eprint.iacr.org/2023/149>
- [9] D. H. Bailey, "FFTs in External or Hierarchical Memory," in *ACM/IEEE Conference on Supercomputing*, 1989, pp. 234–242.
- [10] F. Boemer, S. Kim, G. Seifu, F. D. M. de Souza, and V. Gopal, "Intel HEXL: Accelerating Homomorphic Encryption with Intel AVX512-IFMA52," in *Workshop on Encrypted Computing & Applied Homomorphic Cryptography*, 2021, pp. 57–62.
- [11] J. Bossuat, C. Mouchet, J. R. Troncoso-Pastoriza, and J. Hubaux, "Efficient Bootstrapping for Approximate Homomorphic Encryption with Non-sparse Keys," in *Annual International Conference on the Theory and Applications of Cryptographic Techniques*, 2021, pp. 587–617.
- [12] J. Bossuat, J. Troncoso-Pastoriza, and J. Hubaux, "Bootstrapping for Approximate Homomorphic Encryption with Negligible Failure-Probability by Using Sparse-Secret Encapsulation," in *Applied Cryptography and Network Security*, 2022, pp. 521–541.
- [13] F. Bourse, M. Minelli, M. Minihold, and P. Paillier, "Fast Homomorphic Evaluation of Deep Discretized Neural Networks," in *Annual International Conference*, 2018, pp. 483–512.
- [14] Z. Brakerski, C. Gentry, and V. Vaikuntanathan, "(Leveled) Fully Homomorphic Encryption without Bootstrapping," *ACM Transactions on Computing Theory*, vol. 6, no. 3, pp. 1–36, 2014.
- [15] Z. Brakerski and V. Vaikuntanathan, "Efficient Fully Homomorphic Encryption from (Standard) LWE," *SIAM Journal on Computing*, vol. 43, no. 2, pp. 831–871, 2014.
- [16] L. Cao, "Advanced Packaging Technology Platforms for Chiplets and Heterogeneous Integration," in *International Electron Devices Meeting*, 2022, pp. 3.3.1–3.3.4.
- [17] J. Chang, Y. Chen, W. Chan, S. P. Singh, H. Cheng, H. Fujiwara, J. Lin, K. Lin, J. Hung, R. Lee, H. Liao, J. Liaw, Q. Li, C. Lin, M. Chiang, and S. Wu, "A 7nm 256Mb SRAM in High-K Metal-Gate FinFET Technology with Write-Assist Circuitry for Low-VMIN Applications," in *IEEE International Solid-State Circuits Conference*, 2017, pp. 206–207.

- [18] H. Chen and K. Han, "Homomorphic Lower Digits Removal and Improved FHE Bootstrapping," in *Annual International Conference on the Theory and Applications of Cryptographic Techniques*, 2018, pp. 315–337.
- [19] H. Chen, K. Laine, and R. Player, "Simple Encrypted Arithmetic Library - SEAL v2.1," in *Financial Cryptography and Data Security*, 2017, pp. 3–18.
- [20] J. H. Cheon, K. Han, A. Kim, M. Kim, and Y. Song, "A Full RNS Variant of Approximate Homomorphic Encryption," in *Selected Areas in Cryptography*, 2018, pp. 347–368.
- [21] J. H. Cheon, A. Kim, M. Kim, and Y. S. Song, "Homomorphic Encryption for Arithmetic of Approximate Numbers," in *International Conference on the Theory and Applications of Cryptology and Information Security*, 2017, pp. 409–437.
- [22] I. Chillotti, N. Gama, M. Georgieva, and M. Izabachène, "TFHE: Fast Fully Homomorphic Encryption Over the Torus," *Journal of Cryptology*, vol. 33, no. 1, pp. 34–91, 2020.
- [23] I. Chillotti, M. Joye, and P. Paillier, "Programmable Bootstrapping Enables Efficient Homomorphic Inference of Deep Neural Networks," in *Cyber Security Cryptography and Machine Learning*, 2021, pp. 1–19.
- [24] L. T. Clark, V. Vashishtha, L. Shifren, A. Gujja, S. Sinha, B. Cline, C. Ramamurthy, and G. Yeric, "ASAP7: A 7-nm FinFET Predictive Process Design Kit," *Microelectronics Journal*, vol. 53, pp. 105–115, 2016.
- [25] J. W. Cooley and J. W. Tukey, "An Algorithm for the Machine Calculation of Complex Fourier Series," *Mathematics of Computation*, vol. 19, no. 90, pp. 297–301, 1965.
- [26] CryptoLab Inc., "HEAAN v2.1," Sep 2018. [Online]. Available: <https://github.com/snucrypto/HEAAN>
- [27] B. R. Curtis and R. Player, "On the Feasibility and Impact of Standardising Sparse-secret LWE Parameter Sets for Homomorphic Encryption," in *Workshop on Encrypted Computing & Applied Homomorphic Cryptography*, 2019, pp. 1–10.
- [28] W. Dai and B. Sunar, "cuHE: A Homomorphic Encryption Accelerator Library," in *Cryptography and Information Security in the Balkans*, 2016, pp. 169–186.
- [29] W. J. Dally, "Virtual-Channel Flow Control," *IEEE Transactions on Parallel and Distributed Systems*, vol. 3, no. 2, pp. 194–205, 1992.
- [30] L. Ducas and D. Micciancio, "FHEW: Bootstrapping Homomorphic Encryption in Less Than a Second," in *Annual International Conference on the Theory and Applications of Cryptographic Techniques*, 2015, pp. 617–640.
- [31] EPFL-LDS and Tune Insight SA, "Lattigo v4," Aug 2022. [Online]. Available: <https://github.com/tuneinsight/lattigo>
- [32] J. Fan and F. Vercauteren, "Somewhat Practical Fully Homomorphic Encryption," *Cryptology ePrint Archive*, Paper 2012/144, 2012. [Online]. Available: <https://eprint.iacr.org/2012/144>
- [33] S. Fan, Z. Wang, W. Xu, R. Hou, D. Meng, and M. Zhang, "TensorFHE: Achieving Practical Computation on Encrypted Data Using GPGPU," in *HPCA*, 2023, pp. 922–934.
- [34] S. Halevi and V. Shoup, "Faster Homomorphic Linear Transformations in HELib," in *Annual International Cryptology Conference*, 2018, pp. 93–120.
- [35] K. Han, S. Hong, J. H. Cheon, and D. Park, "Logistic Regression on Homomorphic Encrypted Data at Scale," in *AAAI Conference on Artificial Intelligence*, 2019, pp. 9466–9471.
- [36] K. Han and D. Ki, "Better Bootstrapping for Approximate Homomorphic Encryption," in *Cryptographers' Track at the RSA Conference*, 2020, pp. 364–390.
- [37] M. Han, Y. Zhu, Q. Lou, Z. Zhou, S. Guo, and L. Ju, "coxHE: A Software-Hardware Co-Design Framework for FPGA Acceleration of Homomorphic Computation," in *Design, Automation & Test in Europe Conference & Exhibition*, 2022, pp. 1353–1358.
- [38] S. Hong, S. Kim, J. Choi, Y. Lee, and J. H. Cheon, "Efficient Sorting of Homomorphic Encrypted Data With k-Way Sorting Network," *IEEE Transactions on Information Forensics and Security*, vol. 16, pp. 4389–4404, 2021.
- [39] S. Y. Hou, W. C. Chen, C. Hu, C. Chiu, K. C. Ting, T. S. Lin, W. H. Wei, W. C. Chiou, V. J. C. Lin, V. C. Y. Chang, C. T. Wang, C. H. Wu, and D. Yu, "Wafer-Level Integration of an Advanced Logic-Memory System Through the Second-Generation CoWoS Technology," *IEEE Transactions on Electron Devices*, vol. 64, no. 10, pp. 4071–4077, 2017.
- [40] Z. Huang, W. jie Lu, C. Hong, and J. Ding, "Cheetah: Lean and Fast Secure Two-Party Deep Neural Network Inference," in *USENIX Security Symposium*, 2022, pp. 809–826.
- [41] R. Hwang, T. Kim, Y. Kwon, and M. Rhu, "Centaur: A Chiplet-based, Hybrid Sparse-Dense Accelerator for Personalized Recommendations," in *ISCA*, 2020, pp. 968–981.
- [42] IEEE, "International Roadmap for Devices and Systems," Tech. Rep., 2018. [Online]. Available: <https://irds.ieee.org/editions/2018/>
- [43] IEEE, "Heterogeneous Integration Roadmap," Tech. Rep., 2021. [Online]. Available: <https://eps.ieee.org/technology/heterogeneous-integration-roadmap.html>
- [44] Y. Ishimaki, H. Imabayashi, K. Shimizu, and H. Yamana, "Privacy-Preserving String Search for Genome Sequences with FHE Bootstrapping Optimization," in *2016 IEEE International Conference on Big Data (Big Data)*, 2016, pp. 3989–3991.
- [45] JEDEC, "High Bandwidth Memory (HBM) DRAM," Tech. Rep. JESD235D, 2021.
- [46] JEDEC, "High Bandwidth Memory DRAM (HBM3)," Tech. Rep. JESD238, 2022.
- [47] W. Jeong, S. Maeda, H. Lee, K. Lee, T. Lee, D. Park, B. Kim, J. Do, T. Fukai, D. Kwon, K. Nam, W. Rim, M. Jang, H. Kim, Y. Lee, J. Park, E. Lee, D. Ha, C. Park, H. Cho, S. Jung, and H. Kang, "True 7nm Platform Technology featuring Smallest FinFET and Smallest SRAM cell by EUV, Special Constructs and 3rd Generation Single Diffusion Break," in *IEEE Symposium on VLSI Technology*, 2018, pp. 59–60.
- [48] L. Jiang, Q. Lou, and N. Joshi, "MATCHA: A Fast and Energy-Efficient Accelerator for Fully Homomorphic Encryption over the Torus," in *ACM/IEEE Design Automation Conference*, 2022, pp. 235–240.
- [49] N. P. Jouppi, D. H. Yoon, M. Ashcraft, M. Gottscho, T. B. Jablin, G. Kurian, J. Laudon, S. Li, P. C. Ma, X. Ma, T. Norrie, N. Patil, S. Prasad, C. Young, Z. Zhou, and D. A. Patterson, "Ten Lessons From Three Generations Shaped Google's TPUv4i: Industrial Product," in *ISCA*, 2021, pp. 1–14.
- [50] W. Jung, S. Kim, J. Ahn, J. H. Cheon, and Y. Lee, "Over 100x Faster Bootstrapping in Fully Homomorphic Encryption through Memory-centric Optimization with GPUs," *IACR Transactions on Cryptographic Hardware and Embedded Systems*, vol. 2021, no. 4, pp. 114–148, 2021.
- [51] W. Jung, E. Lee, S. Kim, J. Kim, N. Kim, K. Lee, C. Min, J. H. Cheon, and J. Ahn, "Accelerating Fully Homomorphic Encryption Through Architecture-Centric Analysis and Optimization," *IEEE Access*, vol. 9, pp. 98 772–98 789, 2021.
- [52] C. Juvekar, V. Vaikuntanathan, and A. Chandrakasan, "{GAZELLE}: A Low Latency Framework for Secure Neural Network Inference," in *USENIX Security Symposium*, 2018, pp. 1651–1669.
- [53] A. Kannan, N. E. Jerger, and G. H. Loh, "Enabling Interposer-Based Disintegration of Multi-Core Processors," in *MICRO*, 2015, pp. 546–558.
- [54] J. Kim, G. Lee, S. Kim, G. Sohn, M. Rhu, J. Kim, and J. Ahn, "ARK: Fully Homomorphic Encryption Accelerator with Runtime Data Generation and Inter-Operation Key Reuse," in *MICRO*, 2022, pp. 1237–1254.
- [55] M. Kim, A. O. Harmanci, J.-P. Bossuat, S. Carpov, J. H. Cheon, I. Chillotti, W. Cho, D. Froelicher, N. Gama, M. Georgieva, S. Hong, J.-P. Hubaux, D. Kim, K. Lauter, Y. Ma, L. Ohno-Machado, H. Sofia, Y. Son, Y. Song, J. Troncoso-Pastoriza, and X. Jiang, "Ultrafast homomorphic encryption models enable secure outsourcing of genotype imputation," *Cell Systems*, vol. 12, no. 11, pp. 1108–1120.e4, 2021.
- [56] S. Kim, W. Jung, J. Park, and J. Ahn, "Accelerating Number Theoretic Transformations for Bootstrappable Homomorphic Encryption on GPUs," in *IEEE International Symposium on Workload Characterization*, 2020, pp. 264–275.
- [57] S. Kim, J. Kim, M. J. Kim, W. Jung, J. Kim, M. Rhu, and J. Ahn, "BTS: An Accelerator for Bootstrappable Fully Homomorphic Encryption," in *ISCA*, 2022, pp. 711–725.
- [58] S. Kim, K. Lee, W. Cho, Y. Nam, J. H. Cheon, and R. A. Rutenbar, "Hardware Architecture of a Number Theoretic Transform for a Bootstrappable RNS-based Homomorphic Encryption Scheme," in *IEEE International Symposium on Field-Programmable Custom Computing Machines*, 2020, pp. 56–64.
- [59] T. Kim, Y. Oh, and H. Kim, "Efficient Privacy-Preserving Fingerprint-Based Authentication System Using Fully Homomorphic Encryption," *Security and Communication Networks*, vol. 2020, pp. 1–11, 2020.
- [60] E. Lee, J.-W. Lee, J. Lee, Y.-S. Kim, Y. Kim, J.-S. No, and W. Choi, "Low-Complexity Deep Convolutional Neural Networks on Fully Homomorphic

- Encryption Using Multiplexed Parallel Convolutions,” in *International Conference on Machine Learning*, 2022, pp. 12 403–12 422.
- [61] J.-W. Lee, H. Kang, Y. Lee, W. Choi, J. Eom, M. Deryabin, E. Lee, J. Lee, D. Yoo, Y.-S. Kim, and J.-S. No, “Privacy-Preserving Machine Learning With Fully Homomorphic Encryption for Deep Neural Network,” *IEEE Access*, vol. 10, pp. 30 039–30 054, 2022.
- [62] S. Li, J. Ahn, R. D. Strong, J. B. Brockman, D. M. Tullsen, and N. P. Jouppi, “McPAT: An Integrated Power, Area, and Timing Modeling Framework for Multicore and Manycore Architectures,” in *MICRO*, 2009, pp. 469–480.
- [63] Y. Li, A. Louri, and A. Karanth, “SPACX: Silicon Photonics-based Scalable Chiplet Accelerator for DNN Inference,” in *hPCA*, 2022, pp. 831–845.
- [64] Lotame, “IDFA and Big Tech Impact – One Year Later,” 2022. [Online]. Available: <https://www.lotame.com/idfa-and-big-tech-impact-one-year-later>
- [65] R. Mahajan, R. Sankman, N. Patel, D.-W. Kim, K. Aygun, Z. Qian, Y. Mekonnen, I. Salama, S. Sharan, D. Iyengar, and D. Mallik, “Embedded Multi-die Interconnect Bridge (EMIB) – A High Density, High Bandwidth Packaging Interconnect,” in *IEEE Electronic Components and Technology Conference*, 2016, pp. 557–565.
- [66] A. C. Mert, E. Öztürk, and E. Savaş, “Design and Implementation of a Fast and Scalable NTT-Based Polynomial Multiplier Architecture,” in *Euromicro Conference on Digital System Design*, 2019, pp. 253–260.
- [67] T. Morshed, M. M. A. Aziz, and N. Mohammed, “CPU and GPU Accelerated Fully Homomorphic Encryption,” in *IEEE International Symposium on Hardware Oriented Security and Trust*, 2020, pp. 142–153.
- [68] S. Naffziger, N. Beck, T. Burd, K. Lepak, G. H. Loh, M. Subramony, and S. White, “Pioneering Chiplet Technology and Design for the AMD EPYC™ and Ryzen™ Processor Families : Industrial Product,” in *ISCA*, 2021, pp. 57–70.
- [69] S. Naffziger, K. Lepak, M. Paraschou, and M. Subramony, “AMD Chiplet Architecture for High-Performance Server and Desktop Products,” in *IEEE International Solid-State Circuits Conference*, 2020, pp. 44–45.
- [70] K. Nam, H. Oh, H. Moon, and Y. Paek, “Accelerating N-Bit Operations over TFHE on Commodity CPU-FPGA,” in *IEEE/ACM International Conference on Computer-Aided Design*, 2022, pp. 1–9.
- [71] S. Narasimha, B. Jagannathan, A. Ogino, D. Jaeger, B. Greene, C. Sheraw, K. Zhao, B. Haran, U. Kwon, A. K. M. Mahalingam, B. Kannan, B. Morganfeld, J. Dechene, C. Radens, A. Tessier, A. Hassan, H. Narisetty, I. Ahsan, M. Aminpur, C. An, M. Aquilino, A. Arya, R. Augur, N. Baliga, R. Bhelkar, G. Biery, A. Blauberg, N. Borjemscaia, A. Bryant, L. Cao, V. Chauhan, M. Chen, L. Cheng, J. Choo, C. Christiansen, T. Chu, B. Cohen, R. Coleman, D. Conklin, S. Crown, A. da Silva, D. Dechene, G. Derderian, S. Deshpande, G. Dilliway, K. Donegan, M. Eller, Y. Fan, Q. Fang, A. Gassaria, R. Gauthier, S. Ghosh, G. Gifford, T. Gordon, M. Gribelyuk, G. Han, J. Han, K. Han, M. Hasan, J. Higman, J. Holt, L. Hu, L. Huang, C. Huang, T. Hung, Y. Jin, J. Johnson, S. Johnson, V. Joshi, M. Joshi, P. Justison, S. Kalaga, T. Kim, W. Kim, R. Krishnan, B. Krishnan, K. Anil, M. Kumar, J. Lee, R. Lee, J. Lemon, S. Liew, P. Lindo, M. Lingalugari, M. Lipinski, P. Liu, J. Liu, S. Lucarini, W. Ma, E. Maciejewski, S. Madiseti, A. Malinowski, J. Mehta, C. Meng, S. Mitra, C. Montgomery, H. Nayfeh, T. Nigam, G. Northrop, K. Onishi, C. Ordonio, M. Ozbek, R. Pal, S. Parihar, O. Patterson, E. Ramanathan, I. Ramirez, R. Ranjan, J. Sarad, V. Sardesai, S. Saudari, C. Schiller, B. Senapati, C. Serrau, N. Shah, T. Shen, H. Sheng, J. Shepard, Y. Shi, M. Silvestre, D. Singh, Z. Song, J. Sporre, P. Srinivasan, Z. Sun, A. Sutton, R. Sweeney, K. Tabakman, M. Tan, X. Wang, E. Woodard, G. Xu, D. Xu, T. Xuan, Y. Yan, J. Yang, K. Yeap, M. Yu, A. Zainuddin, J. Zeng, K. Zhang, M. Zhao, Y. Zhong, R. Carter, C. Lin, S. Grunow, C. Child, M. Lagus, R. Fox, E. Kaste, G. Gomba, S. Samavedam, P. Agnello, and D. K. Sohn, “A 7nm CMOS Technology Platform for Mobile and High Performance Compute Application,” in *IEEE International Electron Devices Meeting*, 2017, pp. 29.5.1–29.5.4.
- [72] N. Nassif, A. O. Munch, C. L. Molnar, G. Pasdast, S. V. Lyer, Z. Yang, O. Mendoza, M. Huddart, S. Venkataraman, S. Kandula, R. Marom, A. M. Kern, B. Bowhill, D. R. Mulvihill, S. Nimmagadda, V. Kalidindi, J. Krause, M. M. Haq, R. Sharma, and K. Duda, “Sapphire Rapids: The Next-Generation Intel Xeon Scalable Processor,” in *IEEE International Solid-State Circuits Conference*, vol. 65, 2022, pp. 44–46.
- [73] W. Oed and O. Lange, “On the Effective Bandwidth of Interleaved Memories in Vector Processor Systems,” *IEEE Transactions on Computers*, vol. C-34, no. 10, pp. 949–957, 1985.
- [74] M. O’Connor, N. Chatterjee, D. Lee, J. Wilson, A. Agrawal, S. W. Keckler, and W. J. Dally, “Fine-Grained DRAM: Energy-Efficient DRAM for Extreme Bandwidth Systems,” in *MICRO*, 2017, pp. 41–54.
- [75] G. Pradel and C. Mitchell, “Privacy-Preserving Biometric Matching Using Homomorphic Encryption,” in *IEEE International Conference on Trust, Security and Privacy in Computing and Communications*, 2021, pp. 494–505.
- [76] B. Reagen, W.-S. Choi, Y. Ko, V. T. Lee, H.-H. S. Lee, G.-Y. Wei, and D. Brooks, “Cheetah: Optimizing and Accelerating Homomorphic Encryption for Private Inference,” in *HPCA*, 2021, pp. 26–39.
- [77] O. Regev, “On Lattices, Learning with Errors, Random Linear Codes, and Cryptography,” *Journal of the ACM*, vol. 56, no. 6, pp. 1–40, 2009.
- [78] D. Reis, J. Takeshita, T. Jung, M. Niemier, and X. S. Hu, “Computing-in-Memory for Performance and Energy-Efficient Homomorphic Encryption,” *IEEE Transactions on Very Large Scale Integration Systems*, vol. 28, no. 11, pp. 2300–2313, 2020.
- [79] M. S. Riazi, K. Laine, B. Pelton, and W. Dai, “HEAX: An Architecture for Computing on Encrypted Data,” in *ASPLOS*, 2020, pp. 1295–1309.
- [80] S. S. Roy, F. Turan, K. Järvinen, F. Vercauteren, and I. Verbauwhede, “FPGA-Based High-Performance Parallel Architecture for Homomorphic Computing on Encrypted Data,” in *HPCA*, 2019, pp. 387–398.
- [81] N. Samardzic, A. Feldmann, A. Krastev, S. Devadas, R. Dreslinski, C. Peikert, and D. Sanchez, “F1: A Fast and Programmable Accelerator for Fully Homomorphic Encryption,” in *MICRO*, 2021, pp. 238–252.
- [82] N. Samardzic, A. Feldmann, A. Krastev, N. Manohar, N. Genise, S. Devadas, K. Eldefrawy, C. Peikert, and D. Sanchez, “CraterLake: A Hardware Accelerator for Efficient Unbounded Computation on Encrypted Data,” in *ISCA*, 2022, pp. 173–187.
- [83] G. Seiler, “Faster AVX2 optimized NTT multiplication for Ring-LWE lattice cryptography,” Cryptology ePrint Archive, Paper 2018/039, 2018. [Online]. Available: <https://eprint.iacr.org/2018/039>
- [84] A. Shafaei, Y. Wang, X. Lin, and M. Pedram, “FinCACTI: Architectural Analysis and Modeling of Caches with Deeply-Scaled FinFET Devices,” in *IEEE Computer Society Annual Symposium on VLSI*, 2014, pp. 290–295.
- [85] Y. S. Shao, J. Clemons, R. Venkatesan, B. Zimmer, M. Fojtik, N. Jiang, B. Keller, A. Klinefelter, N. Pinckney, P. Raina, S. G. Tell, Y. Zhang, W. J. Dally, J. Emer, C. T. Gray, B. Khailany, and S. W. Keckler, “Simba: Scaling Deep-Learning Inference with Multi-Chip-Module-Based Architecture,” in *MICRO*, 2019, pp. 14–27.
- [86] T. Song, J. Jung, W. Rim, H. Kim, Y. Kim, C. Park, J. Do, S. Park, S. Cho, H. Jung, B. Kwon, H. Choi, J. Choi, and J. S. Yoon, “A 7nm FinFET SRAM Using EUV Lithography with Dual Write-Driver-Assist Circuitry for Low-Voltage Applications,” in *IEEE International Solid-State Circuits Conference*, 2018, pp. 198–200.
- [87] H. S. Stone, “Parallel Processing with the Perfect Shuffle,” *IEEE Transactions on Computers*, vol. C-20, no. 2, pp. 153–161, 1971.
- [88] E. Talpes, D. D. Sarma, D. Williams, S. Arora, T. Kunjan, B. Floering, A. Jalote, C. Hsiung, C. Poorna, V. Samant, J. Sicilia, A. K. Nivarti, R. Ramachandran, T. Fischer, B. Herzberg, B. McGee, G. Venkataraman, and P. Banon, “The Microarchitecture of DOJO, Tesla’s Exa-Scale Computer,” *IEEE Micro*, pp. 1–5, 2023.
- [89] Z. Tan, H. Cai, R. Dong, and K. Ma, “NN-BATON: DNN Workload Orchestration and Chiplet Granularity Exploration for Multichip Accelerators,” in *ISCA*. IEEE, 2021, pp. 1013–1026.
- [90] F. Turan, S. S. Roy, and I. Verbauwhede, “HEAWS: An Accelerator for Homomorphic Encryption on the Amazon AWS FPGA,” *IEEE Transactions on Computers*, vol. 69, no. 8, pp. 1185–1196, 2020.
- [91] Universal Chiplet Interconnect Express, “Universal Chiplet Interconnect express (UCIe) Specification,” Tech. Rep., 2022. [Online]. Available: <https://www.uciexpress.org/specification>
- [92] Vernam Group, “CUDA-Accelerated Fully Homomorphic Encryption Library,” Feb 2019. [Online]. Available: <https://github.com/vernamlab/cuFHE>
- [93] S. Wu, C. Lin, M. Chiang, J. Liaw, J. Cheng, S. Yang, C. Tsai, P. Chen, T. Miyashita, C. Chang, V. Chang, K. Pan, J. Chen, Y. Mor, K. Lai, C. Liang, H. Chen, S. Chang, C. Lin, C. Hsieh, R. Tsui, C. Yao, C. Chen, R. Chen, C. Lee, H. Lin, C. Chang, K. Chen, M. Tsai, K. Chen, Y. Ku, and S. Jang, “A 7nm CMOS Platform Technology Featuring 4th Generation FinFET Transistors with a 0.027um2 High Density 6-T SRAM cell for Mobile SoC Applications,” in *IEEE International Electron Devices Meeting*, 2016, pp. 2.6.1–2.6.4.

- [94] J. Xia, C. Cheng, X. Zhou, Y. Hu, and P. Chun, "Kunpeng 920: The First 7-nm Chiplet-Based 64-Core ARM SoC for Cloud Services," *IEEE Micro*, vol. 41, no. 5, pp. 67–75, 2021.
- [95] Y. Yang, H. Zhang, S. Fan, H. Lu, M. Zhang, and X. Li, "Poseidon: Practical Homomorphic Encryption Accelerator," in *HPCA*, 2023, pp. 870–881.
- [96] F. Zaruba, F. Schuiki, and L. Benini, "Manticore: A 4096-Core RISC-V Chiplet Architecture for Ultraefficient Floating-Point Computing," *IEEE Micro*, vol. 41, no. 2, pp. 36–42, 2021.
- [97] Y. Zhai, M. Ibrahim, Y. Qiu, F. Boemer, Z. Chen, A. Titov, and A. Lyashevsky, "Accelerating Encrypted Computing on Intel GPUs," in *IEEE International Parallel and Distributed Processing Symposium*, 2022, pp. 705–716.
- [98] Y. Zhu, X. Wang, L. Ju, and S. Guo, "FxHENN: FPGA-based Acceleration Framework for Homomorphic Encrypted CNN Inference," in *HPCA*, 2023, pp. 896–907.